High-Resolution MAS NMR Analysis of PI3-SH3 Amyloid Fibrils: Backbone Conformation and Implications for Protofilament Assembly and Structure

ARTICLE *in* BIOCHEMISTRY · SEPTEMBER 2010

Impact Factor: 3.02 · DOI: 10.1021/bi100864t · Source: PubMed

6 AUTHORS, INCLUDING:

Thorsten Maly
Bridge12 Technologies, Inc.
27 PUBLICATIONS **708** CITATIONS
SEE PROFILE

Neil R Birkett
MedImmune, LLC
9 PUBLICATIONS **275** CITATIONS
SEE PROFILE

Cait Macphee
The University of Edinburgh
74 PUBLICATIONS **3,290** CITATIONS
SEE PROFILE

Robert G Griffin
Massachusetts Institute of Technology
454 PUBLICATIONS **24,789** CITATIONS
SEE PROFILE

Published in final edited form as:
Biochemistry. 2010 September 7; 49(35): 7474–7484. doi:10.1021/bi100864t.

High-resolution MAS NMR analysis of PI3-SH3 amyloid fibrils: Backbone conformation and implications for protofilament assembly and structure

Marvin J. Bayro[a], **Thorsten Maly**[a], **Neil R. Birkett**[b], **Cait E. MacPhee**[c], **Christopher M. Dobson**[b], and **Robert G. Griffin**[a,*]

[a]Francis Bitter Magnet Laboratory and Department of Chemistry, Massachusetts Institute of Technology, Cambridge, MA 02139, USA

[b]Department of Chemistry, University of Cambridge, Lensfield Road, Cambridge, CB2 1EW, UK

[c]SUPA, School of Physics and Astronomy, University of Edinburgh, Edinburgh, EH9 3JZ, UK

Abstract

The SH3 domain of the PI3 kinase (PI3-SH3 or PI3K-SH3) readily aggregates into fibrils *in vitro* and has served as an important model system to investigate the molecular properties and mechanism of formation of amyloid fibrils. We describe the molecular conformation of PI3-SH3 in amyloid fibril form as revealed by magic-angle spinning (MAS) solid-state nuclear magnetic resonance (NMR) spectroscopy. The MAS NMR spectra of these fibrils display excellent resolution, with narrow ^{13}C and ^{15}N line widths, representing a high degree of structural order and the absence of extensive molecular motion for the majority of the polypeptide chain. We have identified the spin-systems of 82 of the 86 residues in the protein, and obtained sequential resonance assignments for 75 of them. Chemical shift analysis indicates that the protein subunits making up the fibril adopt a compact conformation consisting of four well-defined β-sheet regions and four random-coil elements with varying degrees of local dynamics or disorder. The backbone conformation of PI3-SH3 in fibril form differs significantly from that of the native state of the protein, both in secondary structure and in the location of dynamic or disordered segments. The site-specific MAS NMR analysis of PI3-SH3 fibrils we report here is compared with previously published mechanistic and structural data, resulting in a detailed interpretation of the factors that mediate fibril formation by PI3-SH3 and allowing us to propose a possible model of the core structure of the fibrils. Our results confirm the structural similarities between PI3-SH3 fibrils and amyloids directly related to degenerative or infectious diseases.

Amyloid fibrils are filamentous structures resulting from the spontaneous self-assembly of otherwise soluble peptides and proteins (1–4). A large number of human disorders, including Alzheimer's and Parkinson's diseases, type 2 diabetes and a variety of systemic amyloidoses, are associated with the formation of such macromolecular assemblies (1,5,6). In each of these pathological conditions, a specific peptide or protein, or protein fragment,

*Corresponding Author: Robert G. Griffin, Massachusetts Institute of Technology, 170 Albany Street, 02139 Cambridge, MA USA, rgg@mit.edu, Tel.: +1 617-253-5597, Fax: +1 617-253-5404.

Data deposition: Chemical shifts have been deposited into the Biological Magnetic Resonance Bank (BMRB), www.bmrb.wisc.org (BMRB ID 16448).

Supporting Information

Two-dimensional ^{13}C-^{13}C and ^{15}N-^{13}C correlation spectra with complete resonance assignments, chemical shift analysis, detailed TALOS results, images of PDB structures of amyloid fibrils mentioned above and a chemical shift table. These supplemental materials may be accessed free of charge at http://pubs.acs.org

transforms from its usual soluble native form into insoluble amyloid fibrils that can accumulate in a variety of organs and tissues. It is not yet clear, in what manner the process of amyloid fibril formation leads to the pathogenic behavior that characterizes these diseases; however, in the systemic conditions it is likely that the fibrils themselves contribute very significantly to the process of organ damage (5). Furthermore, an increasing number of proteins with no link to deposition diseases have been found to form functional amyloid structures in organisms ranging from bacteria to mammals (7–10).

The mechanisms of amyloid fibril formation, and the structures of the amyloid fibrils themselves, are inherently interesting topics and raise important questions from a physical as well as a biological perspective (11). To explain the molecular basis of amyloid fibril formation by globular proteins, it has been proposed that a critical early step is the partial unfolding of the protein, resulting in flexible conformers that expose aggregation-prone regions of the sequence, which are largely buried in the native state, to the external environment (12). In the example investigated here, fibrils are formed *in vitro* by the SH3 domain of the p85α subunit of bovine phosphatidylinositol 3-kinase (PI3-SH3) under acidic conditions (13). The structure of the protein in its native state is well-characterized by X-ray crystallography (14) and solution NMR spectroscopy (15–17), and studies of the acid unfolded state provide clear evidence that the protein adopts a partially folded conformation prior to fibril formation (13,18). However, to understand in detail the mechanism by which PI3-SH3 fibrils form and to characterize their properties, it is necessary to elucidate the structure of the fibrillar state at atomic resolution. In combination with information available from previous biophysical studies on this system, the characterization of PI3-SH3 fibrils is likely to reveal significant insights into the universal features of amyloid formation and structure (19–23).

Proteins that readily aggregate to form amyloid fibrils do not share any obvious sequence identity or structural homology to one another. Prior to their transformation into fibrils, amyloidogenic proteins can possess a variety of secondary structure elements, but in their fibrillar state, as revealed by X-ray fiber diffraction data, they adopt a cross-β structure, in which arrays of β-strands are oriented approximately perpendicular to the long axis of the fibril. In addition, fibrils from a wide variety of peptides and proteins typically display a long, unbranched and frequently twisted morphology (24), suggesting that the ability to form fibrils is an inherent property of polypeptide chains and not restricted to pathological cases, although the propensity to aggregate and the molecular details of the resulting structures are highly sequence-dependent (1).

The physical properties of amyloid fibrils impede their study by conventional high-resolution structural techniques such as single-crystal X-ray crystallography and solution NMR spectroscopy. Specifically, they do not possess long-range three-dimensional order, do not diffract to high resolution, are typically insoluble, and have high molecular weights. Therefore, the majority of structural information on these species has been obtained through complementary techniques such as transmission electron microscopy, atomic force microscopy, and X-ray fiber diffraction (24–26). In the past decade, however, significant advances in magic angle spinning solid-state NMR (MAS NMR), notably dipolar recoupling methodology, has enabled the *de novo* determination of the structures of complex biological molecules in the solid state. In particular, high-resolution MAS NMR structures have been obtained for short peptides and microcrystalline proteins (27–30) and for an 11-residue fragment of human transthyretin (TTR) in its amyloid fibril form (31,32). Furthermore, detailed structural information, and in some cases structural models, have been obtained by MAS NMR spectroscopy for several amyloid fibrils and prion proteins such as α-synuclein (33), the amyloid-β (Aβ) peptide (34–38), the GNNQQNY fragment of Sup35 (39), β_2-microglobulin (40), HET-s (41) and a fragment of the yeast prion protein Ure2p (42). MAS

NMR experiments based on dipole-dipole interactions permit the analysis of rigid structural domains, such as the core of amyloid fibrils. In addition, the incorporation of techniques originally developed for liquid-state NMR studies into MAS NMR experiments (43) facilitates the analysis of highly flexible regions of the fibril (33,44). Solid-state NMR spectroscopy is therefore a highly versatile method for the study of the structure and dynamics of biological macromolecules, even those as challenging to characterize as amyloid fibrils (45) and other kinds of protein aggregates and assemblies (46–48).

In this article we describe site-specific structural characteristics of PI3-SH3 in amyloid fibril form determined via MAS NMR spectroscopy. The dipolar correlation spectra of PI3-SH3 exhibit excellent resolution, allowing us to identify 82 spin systems for the 86-residue protein. Analysis of samples prepared with alternating ^{13}C-^{12}C labeling (28,49,50) resulted in site-specific assignments for the majority of the ^{13}C and ^{15}N resonances observed. Spectral and chemical shift analyses suggest that the backbone conformation of PI3-SH3 in fibril form consists of well-defined secondary structure elements interrupted by short segments of less regular structure. Interpreting the results from previous structural and mechanistic studies on PI3-SH3, in light of the molecular conformation of the fibril subunits reported here, provides key insights into the process of fibril formation and overall fibril structure. The amyloid characteristics at the molecular level of PI3-SH3 described here are similar to those of disease-associated protein fibrils, and thus strongly support the idea that amyloid fibrils are commonly accessible structural states (1,4) and highlight the importance of studying model systems in order to enhance our understanding of the underlying principles of amyloid assembly and structure.

Materials and Methods

Sample Preparation

The 86-residue, 9.6 kDa PI3-SH3 domain was expressed as a his_6-tag fusion construct in BL21(DE3)pLysS *E. Coli* cells using M9 minimal medium as described previously (13). For uniformly ^{13}C and ^{15}N labeled material (U-PI3-SH3), the medium was supplemented with ^{15}N-ammonium chloride and ^{13}C-glucose as the sole nitrogen and carbon sources. A sample in which ^{13}C is incorporated in approximately every other carbon site (2-PI3-SH3) was prepared using [2-^{13}C]glycerol and $NaH_{13}CO_3$ (Cambridge Isotopes, Andover MA) as the sole sources of carbon (28,49). The protein was isolated by nickel affinity chromatography and further purified by size exclusion chromatography. Fibrils were prepared by incubating 1.0 mM monomeric PI3-SH3 in aqueous solution at pH 2.0 for two to three weeks at 25 °C. The fibril morphology was verified periodically by transmission electron microscopy (TEM). Upon completion of fibril formation into a long, straight morphology, the fibrils were collected from solution by centrifugation. For MAS NMR experiments, the buffer was changed to a 60/40 (w/w) mixture of d_5-glycerol and buffer at pH 2.0, via repeated cycles of centrifugation and re-suspension, prior to an ultracentrifugation step for concentration. The wax-like pellet contained approximately 0.5 mg of fibrils per mg of sample material. Finally the pellet was transferred into a MAS rotor by centrifugation. The samples consisted of approximately 5 and 8 mg of protein packed into 2.5 and 3.2 mm rotors, respectively. Fibril morphology after several weeks of MAS NMR data acquisition was verified via TEM images.

MAS NMR Spectroscopy and Data Analysis

NMR experiments were performed on custom-designed spectrometers (courtesy of D. J. Ruben, Francis Bitter Magnet Laboratory) operating at ^1H Larmor frequencies of 700 and 750 MHz. Experiments at 700 MHz were performed using a Varian 3.2 mm triple-resonance probe (Varian Inc, Palo Alto, CA), while at 750 MHz a Bruker 2.5 mm triple-resonance

probe (Bruker BioSpin, Billerica, MA) was used. The sample temperature was maintained by using a stream of nitrogen gas (2 °C). Correlation experiments utilized ramped cross-polarization (CP) and two-pulse phase modulation (TPPM) heteronuclear decoupling (51), and were performed at MAS frequencies ($\omega_r/2\pi$) between 10.0 and 28.5 kHz. For homonuclear correlation experiments RFDR (52–54), DREAM (55), CMAR (56), and PDSD (57) mixing schemes were used with U-PI3-SH3, while RFDR, PDSD, and BASE RFDR (58) were used with 2-PI3-SH3. CMAR experiments were recorded at $\omega_r/2\pi$ = 28.571 kHz using a ^{13}C r.f. field of $\omega_1/2\pi$ = 100.0 kHz. Broadband RFDR experiments were recorded either at $\omega_r/2\pi$ = 18.182 kHz using ^{13}C $\omega_1/2\pi$ = 40 kHz and high-power ^{1}H decoupling or at $\omega_r/2\pi$ = 28.571 kHz using ^{13}C $\omega_1/2\pi$ = 120 kHz without ^{1}H decoupling during the mixing time. PDSD experiments were recorded at $\omega_r/2\pi$ = 10 to 12.5 kHz, with mixing times between 50 and 300 ms. DREAM correlations over the ^{13}C aliphatic ^{13}C region were recorded at $\omega_r/2\pi$ = 16.667 and 28.571 kHz. Heteronuclear correlations were obtained using SPECIFIC CP (59) and TEDOR (60–62) mixing (1.6 ms and 6.0 ms mixing times). Data collection consisted of 1024 indirect points with increments of 25 μs for homonuclear spectra and 320 indirect points with increments of 80 μs for heteronuclear spectra. DREAM, CMAR, RFDR, and 1.6 ms TEDOR spectra were averaged for approximately 48 hours each, while PDSD, BASE RFDR, NCXCY, and 6 ms TEDOR spectra were averaged for four to five days each. ^{13}C and ^{15}N chemical shifts were indirectly referenced to DSS (63) and liquid ammonia (64), respectively. NMR data were processed using NMRPipe (65) and analyzed with Sparky (T.D. Goddard and D.G. Kneller, SPARKY 3, University of California, San Francisco, USA). Secondary structure elements were predicted by calculating the chemical shift deviation from random coil values (66) using the secondary shift values listed by Zhang et al. (67). Backbone torsion angles φ and ψ were predicted with the TALOS program (68), version 2007.068.09.07.

Results

Fibril Homogeneity and Spectral Quality

Amyloid fibrils formed by PI3-SH3 adopt preferentially a single morphology, and are remarkably stable (23). No signals from monomeric PI3-SH3 were observed in MAS NMR spectra. Furthermore, the five samples employed in our analysis show exclusively a single set of chemical shifts and no significant variations in resonance positions were evident between the five different preparations. A second form, uniquely observed in a sixth sample, showed some differences from the first form generated under apparently identical conditions, but was not pursued further in this study, which focuses solely on the first, dominant form.

One-dimensional (1D) MAS NMR spectra of PI3-SH3 fibrils are of very high resolution and permit the observation of important structural features. Two spectra of uniformly labeled PI3-SH3 (U-PI3-SH3) are shown in Figure 1, a direct-detected ^{13}C MAS spectrum (top) and a ^{1}H-^{13}C CP MAS spectrum (bottom). These two spectra are remarkably similar to each other in most of their salient features, the only exception being slightly different intensities for a small number of side-chain resonances. This finding indicates that the protein backbone in PI3-SH3 is in a well defined conformation such that CP enhancement is essentially uniform throughout the polypeptide chain. Indeed, MAS NMR spectra of PI3-SH3 utilizing the INEPT method, aimed at selectively exciting ^{13}C sites in highly flexible regions, yield no protein signals in the temperature range explored in these studies (−10°C to 25°C). CP spectra at various temperatures are shown in Figure S1 of the supporting information. The absence of highly mobile carbon sites, and the close similarity between the CP and the direct ^{13}C polarization spectra, indicate that the majority of the PI3-SH3 polypeptide chain adopts a very rigid conformation in its fibrillar state, in contrast to observations for several other fibrillar systems studied recently, such as α-synuclein (33),

Het-s (44), and a human prion protein (69), where the constituent protein subunits are observed to have both rigid and mobile segments.

A very high degree of structural homogeneity is clearly evident from the 2D ^{13}C-^{13}C correlation spectra of U-PI3-SH3, as illustrated in Figures 2 and 3. The average ^{13}C linewidth is less than 0.5 ppm (94 Hz at a ^{1}H Larmor frequency of 750 MHz), comparable to that observed in uniformly labeled microcrystalline proteins (28, 29, 70–72). Since the spectral resolution of fibril samples depends on their hydration levels (73), PI3-SH3 fibrils were dispersed in a glycerol/water mixture (60/40, w/w) prior to recording spectra to inhibit dehydration of the samples by exploiting the low vapor pressure and hygroscopic properties of glycerol. Indeed, MAS NMR spectra of PI3-SH3 fibrils in buffer alone (pH 2.0) show considerably larger linewidths under the same experimental conditions than those of fibrils in the glycerol/water mixture described above (Figure S2), while the chemical shifts show only marginal changes. Besides preventing dehydration, it is also possible that the glycerol solvent, which has a stabilizing effect in protein structure, may restrict motion in the fibrils and thus contribute to increased structural order and result in narrower lines.

MAS NMR spectra with a comparable resolution to those reported here have been observed for a number of amyloid systems, including the TTR fragment mentioned above (31) and the prion protein fragment HET-s (41). However, in other cases the observed linewidths for amyloid fibrils observed in MAS NMR spectra typically vary between 1 and 5 ppm (33,34,39,74). The excellent quality of the dipolar correlation spectra of U-PI3-SH3 is therefore noteworthy, and can be attributed at least in part to careful control of experimental conditions, but is also indicative of the inherent homogeneity of PI3-SH3 fibrils at the molecular level.

Despite the narrow line widths characteristic of PI3-SH3 fibrils, certain regions of the correlation spectra show a significant degree of resonance overlap consistent with localized structural degeneracy. For example, aliphatic ^{13}C-^{13}C correlation spectra exhibit extensive overlap of $^{13}C\alpha$-$^{13}C\beta$ cross-peaks at chemical shift positions typical of Glu/Gln and Asp/Asn residues (marked with boxes in Figure 2). A low degree of chemical shift dispersion is a consequence of limited variability in secondary structure, and thus is likely to be a feature of the spectra of amyloid fibrils as a result of their high β-sheet content. However, it could also be a consequence of a small degree of local disorder.

Site-specific Resonance Assignments of PI3-SH3 Amyloid Fibrils

Using a combination of 2D homonuclear dipolar correlation experiments with short mixing periods (Figures 2, 3, and S3), it was possible to identify 82 ^{13}C spin-systems out of a total of 86 residues, and for the majority of spin systems all the side-chain resonances are observed. A number of sequential connectivities were initially established with heteronuclear NCACX and NCOCX experiments (59) and with homonuclear ^{13}C-^{13}C correlation experiments under weak coupling conditions (75) using the U-PI3-SH3 sample. However, in order to complement and expedite spectral analysis, we exploited the improved resolution of the 2-PI3-SH3 sample relative to the uniformly labeled one, as well its characteristic attenuation of dipolar truncation effects (76). Spectra of 2-PI3-SH3 typically exhibit linewidths below 0.2 ppm (~38 Hz, at a ^{1}H frequency of 750 MHz) for positions without an adjacent ^{13}C label, and linewidths below 0.1 ppm (~19 Hz, at a ^{1}H frequency of 750 MHz) for some side-chain resonances. Sequential inter-residue correlations in 2-PI3-SH3 were established using band-selective radio-frequency dipolar recoupling (BASE RFDR) experiments optimized for aliphatic ^{13}C nuclei and RFDR for broadband carbonyl-aliphatic recoupling. BASE RFDR generates highly sensitive sequential correlations between aliphatic nuclei, as described recently (58). In particular, a large number of $^{13}C\alpha(i)$-$^{13}C\alpha(i\pm1)$ and $^{13}C\alpha(i)$-$^{13}C\beta(i\pm1)$ correlations appear readily in BASE RFDR

spectra of 2-PI3-SH3, which greatly facilitates resonance assignment. A broadband RFDR experiment, optimized for two-bond ^{13}C'(i)-^{13}Cα(i+1) pairs, can also yield highly informative sequential cross-peaks. Figure 4 compares the resonance assignment information available in broadband RFDR experiments on U-PI3-SH3 and 2-PI3-SH3. Both spectra were recorded under similar conditions (17.6 T and $\omega_r/2\pi$ = 28.5 kHz) using RFDR mixing without ^{1}H decoupling and optimized for one-bond transfer (U-PI3-SH3) and two-bond transfer (2-PI3-SH3). Generation and identification of two-bond ^{13}C'(i)-^{13}Cα(i+1) cross-peaks in U-PI3-SH3 at longer mixing times are precluded by dipolar truncation and by overlap with one-bond intra-residue ^{13}C'(i)-^{13}Cα(i) cross-peaks, respectively. The latter are few in 2-PI3-SH3, and thus numerous sequential correlations may be identified, provided that both ^{13}C sites are labeled simultaneously by this alternating labeling scheme, in at least a fraction of the protein sample. PDSD experiments with 200–300 ms mixing times, although less efficient, provide additional corroboration of homonuclear sequential connectivities obtained with BASE RFDR and two-bond RFDR. Heteronuclear sequential correlations were obtained with TEDOR experiments on 2-PI3-SH3, optimized for either one-bond or two-bond mixing. The latter provided numerous ^{15}N(i)-^{13}C(i-1) connectivities that aided the assignment process and corroborated the partial NCXCY assignments obtained with U-PI3-SH3. Figure 5 illustrates several examples of these sequential TEDOR correlations obtained with 2-PI3-SH3. Due to the improved resolution afforded by this sample, multiple ^{15}N(i)-^{13}Cα(i-1) cross-peaks can be resolved and used to expand upon and verify homonuclear sequential correlations. A detailed description of our resonance assignment scheme and analysis of 2D sequential correlations in samples labeled with [2-^{13}C]glycerol will be the subject of a forthcoming publication.

Site-specific resonance assignments were elucidated for 75 residues, located in two large stretches (G1-K18 and L25-G80) of the sequence, thus leaving two small segments of the sequence unassigned, E19-I24 and the C-terminus, R81-S85 with the exception of P86, assigned unambiguously by elimination. Figure 6a shows the amino acid sequence of PI3-SH3, highlighting the residues that have been assigned at least in part. ^{13}C and ^{15}N chemical shifts for all assigned nuclei are provided in Table 1 of the supplementary material.

For several spin-systems identified in ^{13}C-^{13}C dipolar correlation spectra of U-PI3-SH3, it was not possible to establish inter-residue connections in either U-PI3-SH3 or 2-PI3-SH3 samples due to severe overlap of backbone resonances. In some cases, spin systems were ambiguously identified through their characteristic ^{13}C-^{13}C correlations, but did not yield sequential connectivities with sufficient certainty to establish unambiguous assignments.

Secondary Structure and Dynamics

Site-specific analysis of the MAS NMR spectra allows us to elucidate both global and local characteristics of the PI3-SH3 fibril structure. The well-resolved spectra, presenting a unique set of resonances, are consistent with a high degree of structural homogeneity throughout the fibrils, with every residue in the sequence being in a single environment within the fibril. Secondary structure elements were predicted from the difference between the observed ^{13}C and ^{15}N chemical shifts and their random coil values, using the Chemical Shift Index (66,67,77). Here, the quantity $\Delta\delta = \delta^{13}C\alpha - \delta^{13}C\beta$, from Ref. (77), is particularly useful, since the accuracy of chemical shifts obtained by MAS NMR experiments is usually lower than in solution NMR experiments. The results are summarized in Figure 6b and suggest that most residues in the well-ordered segments of the polypeptide chain are in a β-strand conformation. (See Figure S6 for individual secondary shifts.) To supplement these results, backbone torsion angles φ and ψ were predicted from the chemical shifts using the TALOS program (68), as shown in Figure 6c. (See Figure S7 for further details.) The results from this database approach agree closely with the secondary structure predictions from the Chemical Shift Index.

The secondary structure of PI3-SH3 in amyloid fibril state consists of four well-defined segments adopting predominantly β-strand conformations, linked by random coil elements. Chemical shift analysis indicates that three long stretches of residues assume torsion angles consistent with a β-strand secondary structure, namely S2-K17, L26-A41, and E49-T64, in addition to a short fourth segment, T74-Y78. It important to point out that these predictions may be ambiguous, particularly for segments including Gly residues, and additional tertiary constraints are needed to define the location and structure of β-sheets accurately. The residues that connect the first and second β-strand regions (E19-I24) present weak backbone and side-chain signals in MAS NMR spectra, and thus most of them have not been assigned unambiguously. However, based on such spectral characteristics, we can conjecture that this small region of the sequence is not well defined structurally, presenting either dynamic disorder or conformational heterogeneity. The same conclusions can be reached regarding the last six residues of the sequence. On the other hand, the sequence of residues (L42-Q48) between the second and third β-strand regions appears to be a well-structured loop, based on their intense and narrow MAS NMR signals with random-coil chemical shifts. Another region of random-coil chemicals shifts (T65-G73) is observed between the third and fourth β-strand elements. In summary, the majority of residues giving rise to narrow lines in the MAS NMR spectra of PI3-SH3 fibrils appear to be located in β-strands or in relatively short and ordered regions that link these secondary structure elements.

From the absence of any signals detectable by solution-like NMR methods we can conclude that there are no highly flexible regions in the protein backbone of PI3-SH3 in its fibrillar form. In addition to indicating an overall high level of structural homogeneity, the observation of narrow linewidths for the majority of the PI3-SH3 residues when in the fibril state points to the absence of significant dynamic processes on the timescale of the rf irradiation (decoupling and cross polarization) for these residues, which can lead to line broadening and loss of intensity in MAS NMR spectra (78,79). On the other hand, no resonances could be identified for a few residues within the unassigned segments mentioned above, suggesting that such residues could be in regions of the fibril presenting conformational heterogeneity or undergoing local motions on timescales that interfere with the MAS NMR experiments. Such dynamic interference effects could, in principle, be identified through variable temperature experiments over a wide range of temperatures, and such experiments will be reported in future studies. The C-terminal segment I79-S85, part of which presents weak signals in our spectra, is more exposed to the solvent than the rest of the sequence according to H/D exchange data (80). Other residues showing exchange include K36-G37-S38 and G66-E67, possibly due to mobility or to their particular structure. Residues G66-E67 are in random coil conformation and while K36-G37-S38 is part of a β-strand, they may form a bulge exposing their amide protons to the solvent, or they may be flexible sites due to the presence of Gly residues. Weak side-chain resonances of K36 may be evidence of the latter.

Discussion

Comparison with the Native Fold

The native structure of PI3-SH3 is composed of five β-strands forming a β-barrel and a short helixlike turn (14–16). Fiber-diffraction studies suggest that the orientation of the β-strands in PI3-SH3 fibrils is perpendicular to the fibril axis (13,81), a finding inconsistent with the β-barrel architecture of the native fold. Nevertheless, a simple rearrangement of the β-strands in the native PI3-SH3 fold is sufficient to account for electron-density maps from cyro-EM and thus satisfy the above observation. A comparison of the secondary structure elements of the native PI3-SH3 fold, previously obtained with solution NMR and X-ray crystallography, to those derived from our solid-state NMR chemical shift analysis is depicted in Figure 7, in which bars and cylinders denote β-sheet and helical segments,

respectively, and dashed lines highlight flexible or disordered regions. These plots show that the secondary structure elements in the native fold are significantly different from those elements identified for the protein in the fibril state. The MAS NMR data show that none of the assigned residues adopt α-helical or helix-like conformations in the fibrils, a finding that is in accordance with circular dichroism and FT-IR data (19). More remarkably, β-strand segments are considerably longer in the fibrils than in the native fold.

The secondary structure elements in the native structure of PI3-SH3, as determined by solution NMR spectroscopy (15,16), consist of five β-strands, which are four to six residues in length, and short helical segments. In the native PI3-SH3 fold, the first six N-terminal residues are disordered and the first β-strand is formed by Q9-A12, which is followed by a long random coil segment that includes the RT loop (L13-D25) and the diverging turn (L26-D30). The second β-strand consists of residues I31-V34 and is followed by a flexible stretch of ~22 residues in random coil conformation (referred to as the N-src loop), including a short helical segment and a solvent-exposed helical turn (K51-E54). A well defined type I β turn (E63-G66) links the third and fourth β-strands, composed of residues W57-N62 and E67-P72, respectively. The fifth β-strand, formed by residues E77-R81A, comes after a short helix-like turn, and is followed by a disordered C-terminus (K82-P86). A very similar native conformation is found in the crystal structure of PI3-SH3, with the major difference being that, as a result of intermolecular packing, the N-src loop and the C-terminus are less flexible and better defined in the crystal structure (14). In turn, these intermolecular interactions in the crystal lattice stabilize the secondary structure elements of native PI3-SH3, whose β-strands are longer by a few residues in the crystal structure than in the solution structure, as shown in Figure 6.

Considering the secondary structure elements in the fibrillar state described in the preceding section, we may highlight the following differences (and a few similarities) between PI3-SH3 fibril subunits and the native fold. Three out of the five native β-strands are preserved in the fibril state, as part of longer β-strand elements, while residues that form part of β-strands 4 and 5 in the native state (near the C-terminus) adopt mostly a random-coil conformation in the fibril. The natively disordered N-terminus adopts a rigid β-strand structure in the fibril state, while the native structure's diverging turn goes from a well-defined loop conformation to a β-strand configuration. Similar changes occur for the natively flexible N-src loop region, which encompasses both helical and random-coil residues in the native fold but constitutes the middle of a long, rigid strand-loop-strand region in the fibril state, as shown in Figure 6d. On the other hand, the C-terminal residues, highly flexible in the solution structure, appear to also be dynamically/structurally disordered in the fibrils. Finally, the natively random-coil RT-loop constitutes, in the fibril state, both part of a rigid β-strand region (on the N-terminal side) and a disordered segment with few observed MAS NMR signals.

Our observations therefore demonstrate that PI3-SH3 subunits in amyloid fibrils adopt a conformation that is vastly different from that of the native structure of the protein. While fibril measurements by X-ray and cryo-EM (20) can be rationalized with changes in the relative location of secondary structure elements, our data indicate that, in the case of PI3-SH3, only a few residues preserve their conformations between the native and the fibril state, while the majority of the sequence presents important differences in secondary structure and/or dynamics between one state and the other.

Aggregation Propensity and Fibril Conformation

PI3-SH3 has been thoroughly studied as a model for the characterization of amyloid fibril formation by a natively globular protein, starting from the acid-unfolded state. In particular, multiple studies have shed light on this protein's propensity to form fibrils as a function of

its amino acid sequence and variants thereof, which has led to the identification of key positions in the sequence in which amino acid substitutions may either disrupt or accelerate the aggregation of monomers into amyloid fibrils, as well as segments that have little effect on fibril formation. For example, preparation of chimeras between PI3-SH3 and spectrin-SH3 (SPC-SH3), a structurally homologous protein that does not form fibrils in all conditions tested, showed that the N-src loop does not have an effect on the aggregation propensity of either protein (82), even though it is the most dissimilar region between the two native structures, being much longer and flexible in PI3-SH3. On the other hand, a short segment from the RT-loop and diverging turn regions of PI3-SH3, D23-L28, was sufficient to confer a SPC-SH3 chimera the ability to form amyloid fibrils, suggesting that this part of the sequence of PI3-SH3 has a specific role in its aggregation ability (83). Additional sets of mutations containing at least one residue in this segment were investigated with the aim of exploring the dependence of PI3-SH3 aggregation on three key physico-chemical characteristics of polypeptides, charge, hydrophobicity, and secondary structure tendency (84). The incorporation of extra charges (at pH 2.0) in this region effectively precluded the formation of aggregates, while increasing the polypeptide's helical propensity had a moderate but noticeable effect on disrupting fibril formation (83). Placing charges in regions of the sequence other than the RT-loop/DT segment can also have dramatic effects. As reported recently (85), E54K and E63K single-mutants have elongation rates several orders of magnitude slower than wild-type PI3-SH3, starting with pre-formed fibrils. These two sites, as well as the RT-loop/DT segment, are located near residue stretches that are found to be prone to aggregation, as calculated by the Zyggregator algorithm (86,87), to which their strong influence has been attributed. Moreover, mutation of a charged residue to a neutral one at pH 2.0 (K18Q) resulted in a two-fold increase in the rate of elongation of pre-formed fibrils (85). On the other hand, inserting multiple charges at the N-terminus (via a His-tag) did not interfere significantly with PI3-SH3 aggregation (83), further illustrating the sequence dependence of the factors influencing fibril formation by proteins.

Knowing the secondary structure that the PI3-SH3 polypeptide adopts in fibril form, we can discuss the previously published results described above in the context of both aggregation propensity of the amino acid sequence and the final fibril conformation, which are compared in Figure 7. The RT-loop/DT segment D23-L28 is at the edge of a β-sheet in the fibril conformation that coincides well with a predicted aggregation-prone region in the unfolded state of PI3-SH3 at pH 2.0 (85), which may explain its fundamental role in fibril formation. Conversely, mutated residues near the aggregation-prone segments, such as L28K and D25R (83), may act as "gatekeepers" that prevent intermolecular association and formation of ordered β-sheets via electrostatic charges (88,89). Similarly, residues E54 and E63 flank a predicted aggregation-prone region and, moreover, adopt a β-sheet conformation in the final fibril state, as part of a β-strand spanning residues 49 to 64. The relative location of these residues within the fibril β-strand, with E63 being more peripheral, may account for the slower elongation rate of the E54K mutant compared to E63K fibrils (85), while both are orders of magnitude slower than the wild-type case. A different situation is observed for residues K17 and K18, which are distant from calculated aggregation-prone regions and are not effective gatekeepers, even though they end up being adjacent to a β-sheet segment in the fibril state. These observations support the hypothesis that gatekeeper residues can be found in close proximity to calculated aggregation-prone regions in native or unfolded states and are not restricted to positions within β-sheet segments in the mature fibril state. Indeed, several charged residues are incorporated in the highly ordered β-sheets of the fibril conformation of wild-type PI3-SH3 described in Figure 6. Therefore, the ability of charged residues (and additional charges) to disrupt the aggregation process is highly dependent on their position in the sequence, and not only on the conformation they adopt in the fibril state, which may reflect the specific role they play in the assembly mechanism.

On the Mechanism of PI3-SH3 Fibril Formation

It is interesting to compare our results to published work that addresses directly the mechanism of fibril formation by PI3-SH3. A recent study (80) has shown, via a pulse-labeling hydrogen-deuterium (H/D) exchange technique, that the segments A12-K18 and E21-G29 are the most protected from exchange in mature fibrils formed at pH 2.0, which we have analyzed here. A similar region, Y14-I24, is the most protected in the pre-fibrillar aggregates observed at pH 1.5, a condition found to favor the stabilization of PI3-SH3 intermediates, while other regions have dissimilar levels of exchange for the two species. Furthermore, as the aggregates mature into fibrils at pH 1.5, the H/D profile changes into one that similar to those of mature fibrils at pH 2.0, pointing to a common fibril assembly process in which pre-fibrillar intermediates are formed first and subsequently rearrange into the final fibril structure. This observation is consistent with the nucleated conformational conversion (NCC) mechanism (90), in which monomers in solution coalesce into amorphous oligomers that later undergo reorganizations that produce ordered oligomers and finally amyloid fibrils rich in β-sheets. Indeed, the formation of amyloidogenic oligomers in the process of fibril formation at pH 2.0 has been detected and quantified by a single-molecule fluorescence study (91). The partial protection from H/D exchange in PI3-SH3 intermediates indicates a significant degree of intermolecular organization, which is preserved and extended in the mature fibrils to most residues in the stretch A12-G29. Notably, these protected residues include the mutation-sensitive RT-loop/DT segment D23-L28 as well as part of the N-terminal β-strand of the fibril state. However, while the latter segment (A12-K18) is well ordered according to our MAS NMR data, several residues within the protected segment present weak NMR signals consistent with local structural disorder, namely residues E19 to I24, as described above. Therefore, while residues 12 to 29 are part of a highly persistent structure in the oligomeric intermediates that drive the initial steps of fibril formation, and remain within the core of mature fibrils, our MAS NMR analysis shows that only some of them adopt a highly ordered β-sheet conformation in the final fibril state.

These observations provide further insight into the different functions that distinct segments of the PI3-SH3 sequence may assume during the course of aggregation and fibril elongation. Residues 23 to 28, DIDLHL, present a binary hydrophilic-hydrophobic pattern that has been shown to promote aggregation in various proteins (92,93) and may be responsible for the coalescence of partially ordered oligomers starting from unfolded PI3-SH3 monomers. The few preceding residues (17 to 22, KKEREE), on the other hand, are hydrophilic and positively charged at pH 2.0, yet they do not interfere with aggregation and are partially protected from H/D exchange in both oligomers and fibrils. Finally, residues on both sides of the protected region form β-sheets in the fibril structure (β-strands 1 and 2 in Figure 6), including the segment Y14-K17, which is already protected in the oligomeric intermediates. While there are several aggregation-prone regions in the PI3-SH3 sequence, one in particular (near the DT) seems to be sufficient to cause aggregation and form oligomers and eventually fibrils, in a process consistent with the NCC mechanism. These initial interactions are then likely superseded by their reorganization and the formation of well-ordered β-sheets throughout the remainder of the sequence, as revealed by the MAS NMR measurements presented here.

Implications for a Structural Model

The MAS NMR analysis described above confirms that PI3-SH3 fibrils contain extensive regions of β-structure, as do fibrils associated with degenerative or infectious diseases. In early studies, analysis of FT-IR (19) and cryo-EM data (20) have indicated that approximately ~40% of the PI3-SH3 protein sequence is contained within the fibril β-sheet core, while the remainder of the protein sequence was proposed to form connecting loops and turns within the fibril structure (19). This picture is broadly consistent with our results

that indicate that up to 55% of the PI3-SH3 peptide chain is likely to be in well structured, predominantly β-strand conformations, although the fraction that adopts the cross-β structure characteristic of amyloid fibrils could be somewhat lower.

Our site-specific secondary structure assignments for PI3-SH3 fibrils are in good agreement with previous H/D exchange experiments, which show that most of the amide hydrogen atoms in the fibril structure are significantly protected from solvent exchange (23). Although certain regions of the PI3-SH3 polypeptide chain in the fibril such as charged side-chain residues show evidence of limited dynamics, the absence of segments with liquid-like dynamics is consistent with a compact structure, and with the finding that none of the sequence is susceptible to ready degradation by proteolytic enzymes in the fibril state (22). Thus we can infer that, while the well-structured regions of PI3-SH3 form the core amyloid structure and rigid loops, the remaining segments of the peptide backbone are also packed tightly within the quaternary structure of the fibril.

These results, in combination with structural information for PI3-SH3 previously obtained by cryo-EM, allow us to propose a structural *model* for PI3-SH3 that describes a possible arrangement of the subunit strands within the fibril core. However, we wish to emphasize that this model requires validation, and needs to be refined with additional structural constraints, specifically, interatomic distances and torsion angles that are presently in progress. Nevertheless, we can suggest a possible arrangement of the protein subunits within the fibril architecture given the following facts. (1) Cryo-EM data show that the width of the protofilaments composing the fibrils is ~20 Å, sufficient to accommodate two β-sheets, while X-ray diffraction data suggest that the sheet spacing is 9.4 Å (13,20). The fibril cross-section according to cryo-EM consists of four areas of highest electron density that were interpreted as the positions of the β-sheets forming the fibril core, while areas of diffuse electron density form a ring-like structure and were interpreted as arising from less ordered parts of the fibrils. (2) No peak doubling is observed in our NMR spectra, indicating that all subunits must reside in identical environments, with the lowest symmetry axis for two sheets being a C_2 axis. (3) H/D exchange measurements show that the C-terminus has a slightly higher exchange rate compared to the rest of the sequence in the fibrils (80), which is consistent with our observation of a disordered C-terminus. (4) A tandem repeat of PI3-SH3 has been observed to form fibrils with a macroscopic morphology similar to those formed by the single-domain protein, but apparently composed of two laterally aligned protofilaments (94).

Analyzing the structural data currently available from models of amyloid fibrils (32,95,96) we estimated different averages for the length-per-residue of the β-strands, between ~3.2 Å/residue for straight β-strands and ~2.2 Å/residue for curved β-strands (see supporting information). For PI3-SH3 fibrils three sections of β-strands composed of ~16 residues are predicted by our chemical shift analysis. We note that these lengths are greater than most β-strands which typically contain up to ~10 residues in soluble proteins. With a lower and upper length limit of 2.2 to 3.2 Å/residue the individual β-strands would be between 35 and 51 Å long. However, since chemical shift analysis is only approximate, it would not be surprising if addition of structural constraints resulted in shorter β-strands in a calculated NMR structure. Cryo-EM data show a distance of ~42 Å between the regions of highest electron density in the fibril cross-section, which may correspond to the location of tightly packed β-sheets. This leads to the suggestion that in the case of PI3-SH3 fibrils the β-strands in the fibril core may be arranged in long arches across the fibril cross-section. These qualitative constraints then permit only a few possible arrangements, with one possibility illustrated in Figure 8. In this structural *model*, four β-sheets form the core of each individual protofilament, while lateral interactions between subunits in adjacent protofilaments bring

them together to form the fibrils. Further experimental data will be necessary to test this hypothetical model.

Conclusions

The success of our MAS NMR experiments in achieving almost complete assignment of ^{13}C and ^{15}N resonances of PI3-SH3 in amyloid fibril state, along with the identification of the majority of backbone torsion angles, suggest that a complete solid-state NMR structure of PI3-SH3 amyloid fibrils is within reach. As an alternative route, combination of our initial results with further analysis of chemical shifts (97) and cryo-EM data may lead to a detailed molecular description of the structure of a natively stable protein after conversion into the generic amyloid state. But even prior to a full structure, the present data have provided key information about the local conformation adopted by PI3-SH3 in amyloid fibril form. Solid-state NMR measurements have revealed a high degree of molecular organization in the structure and shown how the secondary structure elements in the amyloid fibril differ from those in the native structure. Our observations in PI3-SH3 reinforce the idea that the main chain preferences for a given type of secondary structure in the native state are not sufficient to determine those of the fibrillar state, but instead, intermolecular and quaternary interactions must guide the conformation of a protein as it is incorporated in amyloid fibrils. The identification of the backbone conformation of PI3-SH3 in the fibril state has allowed us to interpret the results of previous mechanistic studies in terms of site-specific molecular structure and propose a model of protofilament assembly, thus contributing to the further understanding of the complex mechanism of fibril formation by a natively folded protein.

Supplementary Material

Refer to Web version on PubMed Central for supplementary material.

Acknowledgments

The authors acknowledge stimulating conversations with Patrick van der Wel, Galia Debelouchina, Vikram Bajaj, Gaël de Paëpe, Astrid Sivertsen, Matthew Eddy, Jozef Lewandowski, Marc Caporini, and Michele Vendruscolo. T.M. thanks the Deutsche Forschungs Gesellschaft (DFG) for a Postdoctoral Fellowship.

FUNDING: This work was supported by the National Institute of Health (Grants EB-003151 and EB-002026) and the Leverhulme and Wellcome Trusts.

Abbreviations

CP	Cross polarization
CSI	Chemical shift index
MAS	Magic-angle spinning
PDSD	Proton-driven spin diffusion
PI3-SH3	SH3 domain of the p85α subunit of bovine phosphatidylinositol 3-kinase
RFDR	Radio frequency-driven recoupling
TALOS	Torsion angle likelihood obtained from shift and sequence similarity
TEDOR	Transferred echo double resonance

References

1. Chiti F, Dobson CM. Protein misfolding, functional amyloid, and human disease. Annu. Rev. Biochem. 2006; 75:333–366. [PubMed: 16756495]
2. Sipe JD. Amyloidosis. Annu. Rev. Biochem. 1992; 61:947–975. [PubMed: 1497327]
3. Sunde M, Blake CC. From the globular to the fibrous state: protein structure and structural conversion in amyloid formation. Q. Rev. Biophys. 1998; 31:1–39. [PubMed: 9717197]
4. Chiti F, Dobson CM. Amyloid formation by globular proteins under native conditions. Nat. Chem. Biol. 2009; 5:15–22. [PubMed: 19088715]
5. Sacchettini JC, Kelly JW. Therapeutic Strategies for Human Amyloid Diseases. Nat. Rev. Drug Discovery. 2002; 1:267–275.
6. Dobson CM. Protein folding and misfolding. Nature. 2003; 426:884–890. [PubMed: 14685248]
7. Si K, Lindquist S, Kandel ER. A neuronal isoform of the aplysia CPEB has prion-like properties. Cell. 2003; 115:879–891. [PubMed: 14697205]
8. Coustou V, Deleu C, Saupe S, Begueret J. The protein product of the het-s heterokaryon incompatibility gene of the fungus Podospora anserina behaves as a prion analog. Proc. Natl. Acad. Sci. U.S.A. 1997; 94:9773–9778. [PubMed: 9275200]
9. Chapman MR, Robinson LS, Pinkner JS, Roth R, Heuser J, Hammar M, Normark S, Hultgren SJ. Role of Escherichia coli curli operons in directing amyloid fiber formation. Science. 2002; 295:851–855. [PubMed: 11823641]
10. Berson JF, Theos AC, Harper DC, Tenza D, Raposo G, Marks MS. Proprotein convertase cleavage liberates a fibrillogenic fragment of a resident glycoprotein to initiate melanosome biogenesis. J. Cell Biol. 2003; 161:521–533. [PubMed: 12732614]
11. Knowles TP, Fitzpatrick AW, Meehan S, Mott HR, Vendruscolo M, Dobson CM, Welland ME. Role of intermolecular forces in defining material properties of protein nanofibrils. Science. 2007; 318:1900–1903. [PubMed: 18096801]
12. Uversky VN, Fink AL. Conformational constraints for amyloid fibrillation: the importance of being unfolded. Biochim. Biophys. Acta. 2004; 1698:131–153. [PubMed: 15134647]
13. Guijarro JI, Sunde M, Jones JA, Campbell ID, Dobson CM. Amyloid Fibril Formation by an SH3 Domain. Proc. Natl. Acad. Sci. U.S.A. 1998; 95:4224–4228. [PubMed: 9539718]
14. Liang J, Chen JK, Schreiber ST, Clardy J. Crystal structure of PI3K SH3 domain at 2.0 angstroms resolution. J. Mol. Biol. 1996; 257:632–643. [PubMed: 8648629]
15. Booker GW, Gout I, Downing AK, Driscoll PC, Boyd J, Waterfield MD, Campbell ID. Solution structure and ligand-binding site of the SH3 domain of the p85 alpha subunit of phosphatidylinositol 3-kinase. Cell. 1993; 73:813–822. [PubMed: 7684655]
16. Koyama S, Yu H, Dalgarno DC, Shin TB, Zydowsky LD, Schreiber SL. Structure of the PI3K SH3 domain and analysis of the SH3 family. Cell. 1993; 72:945–952. [PubMed: 7681364]
17. Koyama S, Yu H, Dalgarno D, Shin T, Zydowsky L, Schreiber S. 1H and 15N assignments and secondary structure of the PI3K SH3 domain. FEBS Lett. 1993; 324:93–98. [PubMed: 7684988]
18. Ahn HC, Le YT, Nagchowdhuri PS, Derose EF, Putnam-Evans C, London RE, Markley JL, Lim KH. NMR characterizations of an amyloidogenic conformational ensemble of the PI3K SH3 domain. Protein Sci. 2006; 15:2552–2557. [PubMed: 17001038]
19. Zurdo J, Guijarro JI, Dobson CM. Preparation and characterization of purified amyloid fibrils. J. Am. Chem. Soc. 2001; 123:8141–8142. [PubMed: 11506581]
20. Jimenez J, Guijarro J, Orlova E, Zurdo J, Dobson C, Sunde M, Saibil H. Cryo-electron microscopy structure of an SH3 amyloid fibril and model of the molecular packing. EMBO J. 1999; 18:815–821. [PubMed: 10022824]
21. Zurdo J, Guijarro JI, Jimenez JL, Saibil HR, Dobson CM. Dependence on solution conditions of aggregation and amyloid formation by an SH3 domain. J. Mol. Biol. 2001; 311:325–340. [PubMed: 11478864]
22. Polverino de Laureto P, Taddei N, Frare E, Capanni C, Costantini S, Zurdo J, Chiti F, Dobson CM, Fontana A. Protein aggregation and amyloid fibril formation by an SH3 domain probed by limited proteolysis. J. Mol. Biol. 2003; 334:129–141. [PubMed: 14596805]

23. Carulla N, Caddy GL, Hall DR, Zurdo J, Gairi M, Feliz M, Giralt E, Robinson CV, Dobson CM. Molecular recycling within amyloid fibrils. Nature. 2005; 436:554–558. [PubMed: 16049488]
24. Sunde M, Serpell LC, Bartlam M, Fraser PE, Pepys MB, Blake CC. Common core structure of amyloid fibrils by synchrotron X-ray diffraction. J. Mol. Biol. 1997; 273:729–739. [PubMed: 9356260]
25. Serpell LC, Sunde M, Benson MD, Tennent GA, Pepys MB, Fraser PE. The protofilament substructure of amyloid fibrils. J. Mol. Biol. 2000; 300:1033–1039. [PubMed: 10903851]
26. Harper JD, Lieber CM, Lansbury PT Jr. Atomic force microscopic imaging of seeded fibril formation and fibril branching by the Alzheimer's disease amyloid-beta protein. Chem. Biol. 1997; 4:951–959. [PubMed: 9427660]
27. Rienstra CM, Tucker-Kellogg L, Jaroniec CP, Hohwy M, Reif B, McMahon MT, Tidor B, Lozano-Perez T, Griffin RG. De novo determination of peptide structure with solid-state magic-angle spinning NMR spectroscopy. Proc. Natl. Acad. Sci. U.S.A. 2002; 99:10260–10265. [PubMed: 12149447]
28. Castellani F, van Rossum B, Diehl A, Schubert M, Rehbein K, Oschkinat H. Structure of a protein determined by solid-state magic-angle-spinning NMR spectroscopy. Nature. 2002; 420:98–102. [PubMed: 12422222]
29. Zech SG, Wand AJ, McDermott AE. Protein structure determination by high-resolution solid-state NMR spectroscopy: application to microcrystalline ubiquitin. J. Am. Chem. Soc. 2005; 127:8618–8626. [PubMed: 15954766]
30. Loquet A, Bardiaux B, Gardiennet C, Blanchet C, Baldus M, Nilges M, Malliavin T, Bockmann A. 3D Structure Determination of the Crh Protein from Highly Ambiguous Solid-State NMR Restraints. J. Am. Chem. Soc. 2008; 130:3579–3589. [PubMed: 18284240]
31. Jaroniec CP, MacPhee CE, Astrof NS, Dobson CM, Griffin RG. Molecular conformation of a peptide fragment of transthyretin in an amyloid fibril. Proc. Natl. Acad. Sci. U.S.A. 2002; 99:16748–16753. [PubMed: 12481032]
32. Jaroniec CP, MacPhee CE, Bajaj VS, McMahon MT, Dobson CM, Griffin RG. High-resolution molecular structure of a peptide in an amyloid fibril determined by magic angle spinning NMR spectroscopy. Proc. Natl. Acad. Sci. U.S.A. 2004; 101:711–716. [PubMed: 14715898]
33. Heise H, Hoyer W, Becker S, Andronesi OC, Riedel D, Baldus M. Molecular-level secondary structure, polymorphism, and dynamics of full-length alpha-synuclein fibrils studied by solid-state NMR. Proc. Natl. Acad. Sci. U.S.A. 2005; 102:15871–15876. [PubMed: 16247008]
34. Balbach JJ, Ishii Y, Antzutkin ON, Leapman RD, Rizzo NW, Dyda F, Reed J, Tycko R. Amyloid fibril formation by A beta 16–22, a seven-residue fragment of the Alzheimer's beta-amyloid peptide, and structural characterization by solid state NMR. Biochemistry. 2000; 39:13748–13759. [PubMed: 11076514]
35. Antzutkin ON, Leapman RD, Balbach JJ, Tycko R. Supramolecular structural constraints on Alzheimer's beta-amyloid fibrils from electron microscopy and solid-state nuclear magnetic resonance. Biochemistry. 2002; 41:15436–15450. [PubMed: 12484785]
36. Petkova AT, Leapman RD, Guo Z, Yau WM, Mattson MP, Tycko R. Self-propagating, molecular-level polymorphism in Alzheimer's beta-amyloid fibrils. Science. 2005; 307:262–265. [PubMed: 15653506]
37. Paravastu AK, Petkova AT, Tycko R. Polymorphic fibril formation by residues 10–40 of the Alzheimer's beta-amyloid peptide. Biophys. J. 2006; 90:4618–4629. [PubMed: 16565054]
38. Petkova AT, Yau WM, Tycko R. Experimental constraints on quaternary structure in Alzheimer's beta-amyloid fibrils. Biochemistry. 2006; 45:498–512. [PubMed: 16401079]
39. van der Wel PCA, Lewandowski JR, Griffin RG. Solid-State NMR Study of Amyloid Nanocrystals and Fibrils Formed by the Peptide GNNQQNY from Yeast Prion Protein Sup35p. J. Am. Chem. Soc. 2007; 129:5117–5130. [PubMed: 17397156]
40. Debelouchina GT, Platt GW, Bayro MJ, Radford SE, Griffin RG. Magic angle spinning NMR analysis of beta-2-microglobulin amyloid fibrils in two distinct morphologies. J. Am. Chem. Soc. 2010 In Press.

41. Siemer AB, Ritter C, Ernst M, Riek R, Meier BH. High-resolution solid-state NMR spectroscopy of the prion protein HET-s in its amyloid conformation. Angew. Chem. Int. Ed. 2005; 44:2441–2444.

42. Chan JC, Oyler NA, Yau WM, Tycko R. Parallel beta-sheets and polar zippers in amyloid fibrils formed by residues 10–39 of the yeast prion protein Ure2p. Biochemistry. 2005; 44:10669–10680. [PubMed: 16060675]

43. Andronesi OC, Becker S, Seidel K, Heise H, Young HS, Baldus M. Determination of membrane protein structure and dynamics by magic-angle-spinning solid-state NMR spectroscopy. J. Am. Chem. Soc. 2005; 127:12965–12974. [PubMed: 16159291]

44. Siemer AB, Arnold AA, Ritter C, Westfeld T, Ernst M, Riek R, Meier BH. Observation of highly flexible residues in amyloid fibrils of the HET-s prion. J. Am. Chem. Soc. 2006; 128:13224–13228. [PubMed: 17017802]

45. Tycko R. Molecular structure of amyloid fibrils: insights from solid-state NMR. Q. Rev. Biophys. 2006; 39:1–55. [PubMed: 16772049]

46. Curtis-Fisk J, Spencer RM, Weliky DP. Native conformation at specific residues in recombinant inclusion body protein in whole cells determined with solid-state NMR spectroscopy. J. Am. Chem. Soc. 2008; 130:12568–12569. [PubMed: 18759389]

47. Sivertsen AC, Bayro MJ, Belenky M, Griffin RG, Herzfeld J. Solid-state NMR evidence for inequivalent GvpA subunits in gas vesicles. J. Mol. Biol. 2009; 387:1032–1039. [PubMed: 19232353]

48. Han Y, Ahn J, Concel J, Byeon IL, Gronenborn AM, Yang J, Polenova T. Solid-State NMR Studies of HIV-1 Capsid Protein Assemblies. J. Am. Chem. Soc. 2010; 132:1976–1987. [PubMed: 20092249]

49. LeMaster DM, Kushlan DM. Dynamical mapping of E. coli thioredoxin via 13C NMR relaxation analysis. J. Am. Chem. Soc. 1996; 118:9255–9264.

50. Hong M, Jakes K. Selective and extensive C-13 labeling of a membrane protein for solid-state NMR investigations. J. Biomol. NMR. 1999; 14:71–74. [PubMed: 10382307]

51. Bennett AE, Rienstra CM, Auger M, Lakshmi KV, Griffin RG. Heteronuclear decoupling in rotating solids. J. Chem. Phys. 1995; 103:6951–6958.

52. Bennett AE, Griffin RG, Ok JH, Vega S. Chemical shift correlation spectroscopy in rotating solids: Radio frequency-driven dipolar recoupling and longitudinal exchange. J. Chem. Phys. 1992; 96:8624–8627.

53. Bennett AE, Rienstra CM, Griffiths JM, Zhen W, Lansbury PT Jr, Griffin RG. Homonuclear radio frequency-driven recoupling in rotating solids. J. Chem. Phys. 1998; 108:9463–9479.

54. Bayro MJ, Ramachandran R, Caporini MA, Eddy MT, Griffin RG. Radio frequency-driven recoupling at high magic-angle spinning frequencies: Homonuclear recoupling sans heteronuclear decoupling. J. Chem. Phys. 2008; 128:052321. [PubMed: 18266438]

55. Verel R, Ernst M, Meier BH. Adiabatic dipolar recoupling in solid-state NMR: the DREAM scheme. J. Magn. Reson. 2001; 150:81–99. [PubMed: 11330986]

56. De Paëpe G, Bayro MJ, Lewandowski J, Griffin RG. Broadband homonuclear correlation spectroscopy at high magnetic fields and MAS frequencies. J. Am. Chem. Soc. 2006; 128:1776–1777. [PubMed: 16464061]

57. Szeverenyi NM, Sullivan MJ, Maciel GE. Observation of spin exchange by two-dimensional fourier transform 13C cross polarization-magic-angle spinning. J. Magn. Reson. 1982; 47:462–475.

58. Bayro MJ, Maly T, Birkett NR, Dobson CM, Griffin RG. Long-Range Correlations between Aliphatic 13C Nuclei in Protein MAS NMR Spectroscopy. Angew. Chem. Int. Ed. 2009; 48:5708–5710.

59. Baldus M, Petkova AT, Herzfeld J, Griffin RG. Cross polarization in the tilted frame: assignment and spectral simplification in heteronuclear spin systems. Molecular Physics. 1998; 95:1197–1207.

60. Hing AW, Vega S, Schaefer J. Transferred-echo double-resonance NMR. J. Magn. Reson. 1992; 96:205–209.

61. Michal CA, Jelinski LW. REDOR 3D: Heteronuclear distance measurements in uniformly labeled and natural abundance solids. J. Am. Chem. Soc. 1997; 119:9059–9060.

62. Jaroniec C, Filip C, Griffin R. 3D TEDOR NMR Experiments for the Simultaneous Measurement of Multiple Carbon-Nitrogen Distances in Uniformly 13C,15N-Labeled Solids. J. Am. Chem. Soc. 2002; 124:10728–10742. [PubMed: 12207528]
63. Morcombe CR, Zilm KW. Chemical shift referencing in MAS solid state NMR. J. Magn. Reson. 2003; 162:479–486. [PubMed: 12810033]
64. Harris RK, Becker ED, Cabral de Menezes SM, Goodfellow R, Granger P. NMR nomenclature. Nuclear spin properties and conventions for chemical shifts (IUPAC Recommendations 2001). Pure Appl. Chem. 2001; 73:1795–1818.
65. Delaglio F, Grzesiek S, Vuister GW, Zhu G, Pfeifer J, Bax A. NMRPipe: a multidimensional spectral processing system based on UNIX pipes. J. Biomol. NMR. 1995; 6:277–293. [PubMed: 8520220]
66. Wishart DS, Sykes BD. The 13C chemical-shift index: a simple method for the identification of protein secondary structure using 13C chemical-shift data. J. Biomol. NMR. 1994; 4:171–180. [PubMed: 8019132]
67. Zhang H, Neal S, Wishart DS. RefDB: a database of uniformly referenced protein chemical shifts. J. Biomol. NMR. 2003; 25:173–195. [PubMed: 12652131]
68. Cornilescu G, Delaglio F, Bax A. Protein backbone angle restraints from searching a database for chemical shift and sequence homology. J. Biomol. NMR. 1999; 13:289–302. [PubMed: 10212987]
69. Helmus JJ, Surewicz K, Nadaud PS, Surewicz WK, Jaroniec CP. Molecular conformation and dynamics of the Y145Stop variant of human prion protein in amyloid fibrils. Proc. Natl. Acad. Sci. U.S.A. 2008; 105:6284–6289. [PubMed: 18436646]
70. Igumenova TI, McDermott AE, Zilm KW, Martin RW, Paulson EK, Wand AJ. Assignments of carbon NMR resonances for microcrystalline ubiquitin. J. Am. Chem. Soc. 2004; 126:6720–6727. [PubMed: 15161300]
71. Franks WT, Zhou DH, Wylie BJ, Money BG, Graesser DT, Frericks HL, Sahota G, Rienstra CM. Magic-angle spinning solid-state NMR spectroscopy of the beta1 immunoglobulin binding domain of protein G (GB1): 15N and 13C chemical shift assignments and conformational analysis. J. Am. Chem. Soc. 2005; 127:12291–12305. [PubMed: 16131207]
72. Bockmann A, Lange A, Galinier A, Luca S, Giraud N, Juy M, Heise H, Montserret R, Penin F, Baldus M. Solid state NMR sequential resonance assignments and conformational analysis of the 2×10.4 kDa dimeric form of the Bacillus subtilis protein Crh. J. Biomol. NMR. 2003; 27:323–339. [PubMed: 14512730]
73. Siemer AB, Ritter C, Steinmetz MO, Ernst M, Riek R, Meier BH. 13C, 15N resonance assignment of parts of the HET-s prion protein in its amyloid form. J. Biomol. NMR. 2006; 34:75–87. [PubMed: 16518695]
74. Petkova AT, Ishii Y, Balbach JJ, Antzutkin ON, Leapman RD, Delaglio F, Tycko R. A structural model for Alzheimer's beta -amyloid fibrils based on experimental constraints from solid state NMR. Proc. Natl. Acad. Sci. U.S.A. 2002; 99:16742–16747. [PubMed: 12481027]
75. Seidel K, Lange A, Becker S, Hughes CE, Heise H, Baldus M. Protein solid-state NMR resonance assignments from (C-13, C-13) correlation spectroscopy. Phys. Chem. Chem. Phys. 2004; 6:5090–5093.
76. Bayro MJ, Huber M, Ramachandran R, Davenport TC, Meier BH, Ernst M, Griffin RG. Dipolar truncation in magic-angle spinning NMR recoupling experiments. J. Chem. Phys. 2009; 130:114506. [PubMed: 19317544]
77. Luca S, Filippov DV, van Boom JH, Oschkinat H, de Groot HJ, Baldus M. Secondary chemical shifts in immobilized peptides and proteins: a qualitative basis for structure refinement under magic angle spinning. J. Biomol. NMR. 2001; 20:325–331. [PubMed: 11563556]
78. Long JR, Sun BQ, Bowen A, Griffin RG. Molecular Dynamics and Magic Angle Spinning NMR. J. Am. Chem. Soc. 1994; 116:11950–11956.
79. Maus DC, Copie V, Sun B, Griffiths JM, Griffin RG, Luo S, Schrock RR, Liu AH, Seidel SW, Davis WM, Grohmann A. A Solid-State NMR Study of Tungsten Methyl Group Dynamics in $[W(\bullet^{5}\text{-}C_5Me_5)Me_4][PF_6]$. J. Am. Chem. Soc. 1996; 118:5665–5671.

80. Carulla N, Zhou M, Arimon M, Gairí M, Giralt E, Robinson CV, Dobson CM. Experimental characterization of disordered and ordered aggregates populated during the process of amyloid fibril formation. Proc. Natl. Acad. Sci. U.S.A. 2009; 106:7828–7833. [PubMed: 19416886]
81. Blake C, Serpell L. Synchrotron X-ray studies suggest that the core of the transthyretin amyloid fibril is a continuous [beta]-sheet helix. Structure. 1996; 4:989–998. [PubMed: 8805583]
82. Ventura S, Lacroix E, Serrano L. Insights into the origin of the tendency of the PI3-SH3 domain to form amyloid fibrils. J. Mol. Biol. 2002; 322:1147–1158. [PubMed: 12367534]
83. Ventura S, Zurdo J, Narayanan S, Parreño M, Mangues R, Reif B, Chiti F, Giannoni E, Dobson CM, Aviles FX, Serrano L. Short amino acid stretches can mediate amyloid formation in globular proteins: the Src homology 3 SH3 case. Proc. Natl. Acad. Sci. U.S.A. 2004; 101:7258–7263. [PubMed: 15123800]
84. Chiti F, Stefani M, Taddei N, Ramponi G, Dobson CM. Rationalization of the effects of mutations on peptide and protein aggregation rates. Nature. 2003; 424:805–808. [PubMed: 12917692]
85. Buell AK, Tartaglia GG, Birkett NR, Waudby CA, Vendruscolo M, Salvatella X, Welland ME, Dobson CM, Knowles TP. Position-dependent electrostatic protection against protein aggregation. Chembiochem. 2009; 10:1309–1312. [PubMed: 19415709]
86. Tartaglia GG, Pawar AP, Campioni S, Dobson CM, Chiti F, Vendruscolo M. Prediction of aggregation-prone regions in structured proteins. J. Mol. Biol. 2008; 380:425–436. [PubMed: 18514226]
87. Tartaglia GG, Vendruscolo M. The Zyggregator method for predicting protein aggregation propensities. Chem. Soc. Rev. 2008; 37:1395–1401. [PubMed: 18568165]
88. Otzen DE, Oliveberg M. Salt-induced detour through compact regions of the protein folding landscape. Proc. Natl. Acad. Sci. U.S.A. 1999; 96:11746–11751. [PubMed: 10518521]
89. Matysiak S, Clementi C. Minimalist protein model as a diagnostic tool for misfolding and aggregation. J. Mol. Biol. 2006; 363:297–308. [PubMed: 16959265]
90. Serio TR, Cashikar AG, Kowal AS, Sawicki GJ, Moslehi JJ, Serpell L, Arnsdorf MF, Lindquist SL. Nucleated conformational conversion and the replication of conformational information by a prion determinant. Science. 2000; 289:1317–1321. [PubMed: 10958771]
91. Orte A, Birkett NR, Clarke RW, Devlin GL, Dobson CM, Klenerman D. Direct characterization of amyloidogenic oligomers by single-molecule fluorescence. Proc. Natl. Acad. Sci. U.S.A. 2008; 105:14424–14429. [PubMed: 18796612]
92. West MW, Wang WX, Patterson J, Mancias JD, Beasley JR, Hecht MH. De novo amyloid proteins from designed combinatorial libraries. Proc. Natl. Acad. Sci. U.S.A. 1999; 96:11211–11216. [PubMed: 10500156]
93. Broome BM, Hecht MH. Nature disfavors sequences of alternating polar and non-polar amino acids: Implications for amyloidogenesis. J. Mol. Biol. 2000; 296:961–968. [PubMed: 10686095]
94. Bader R, Bamford R, Zurdo J, Luisi BF, Dobson CM. Probing the mechanism of amyloidogenesis through a tandem repeat of the PI3-SH3 domain suggests a generic model for protein aggregation and fibril formation. J. Mol. Biol. 2006; 356:189–208. [PubMed: 16364365]
95. Wasmer C, Lange A, Van Melckebeke H, Siemer AB, Riek R, Meier BH. Amyloid fibrils of the HET-s(218–289) prion form a beta solenoid with a triangular hydrophobic core. Science. 2008; 319:1523–1526. [PubMed: 18339938]
96. Iwata K, Fujiwara T, Matsuki Y, Akutsu H, Takahashi S, Naiki H, Goto Y. 3D structure of amyloid protofilaments of beta-2-microglobulin fragment probed by solid-state NMR. Proc. Natl. Acad. Sci. U.S.A. 2006; 103:18119–18124. [PubMed: 17108084]
97. Robustelli P, Cavalli A, Vendruscolo M. Determination of protein structures in the solid state from NMR chemical shifts. Structure. 2008; 16:1764–1769. [PubMed: 19081052]

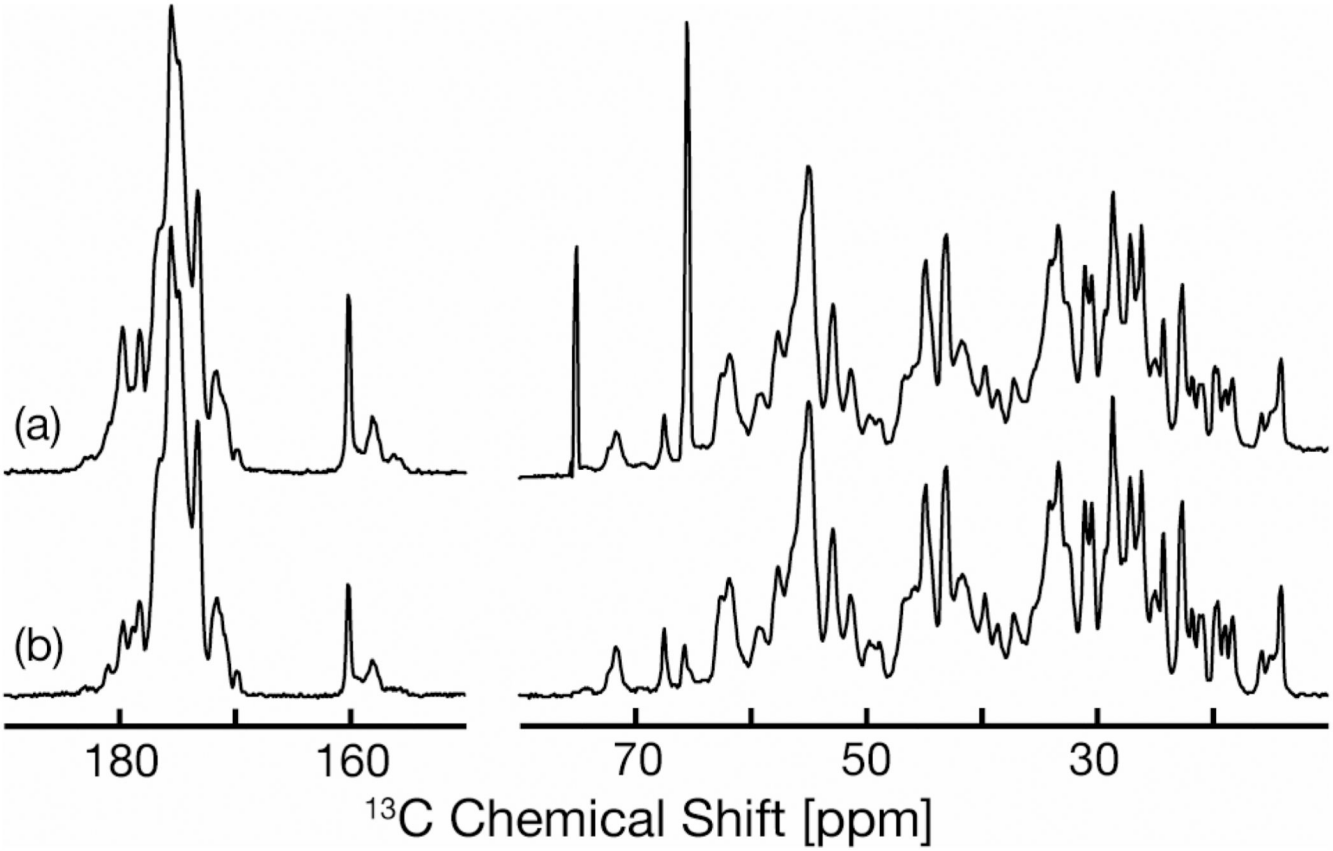

Figure 1.
1D ^{13}C MAS NMR spectra of U-PI3-SH3 fibrils recorded at 750 MHz ^{1}H Larmor frequency and $\omega_r/2\pi$ = 16.67 kHz, at the temperature of 2 °C. (a) Direct ^{13}C spectrum (Bloch decay), scaled by factor of 2.5. (b) ^{13}C cross-polarization spectrum obtained with 1.5 ms contact time.

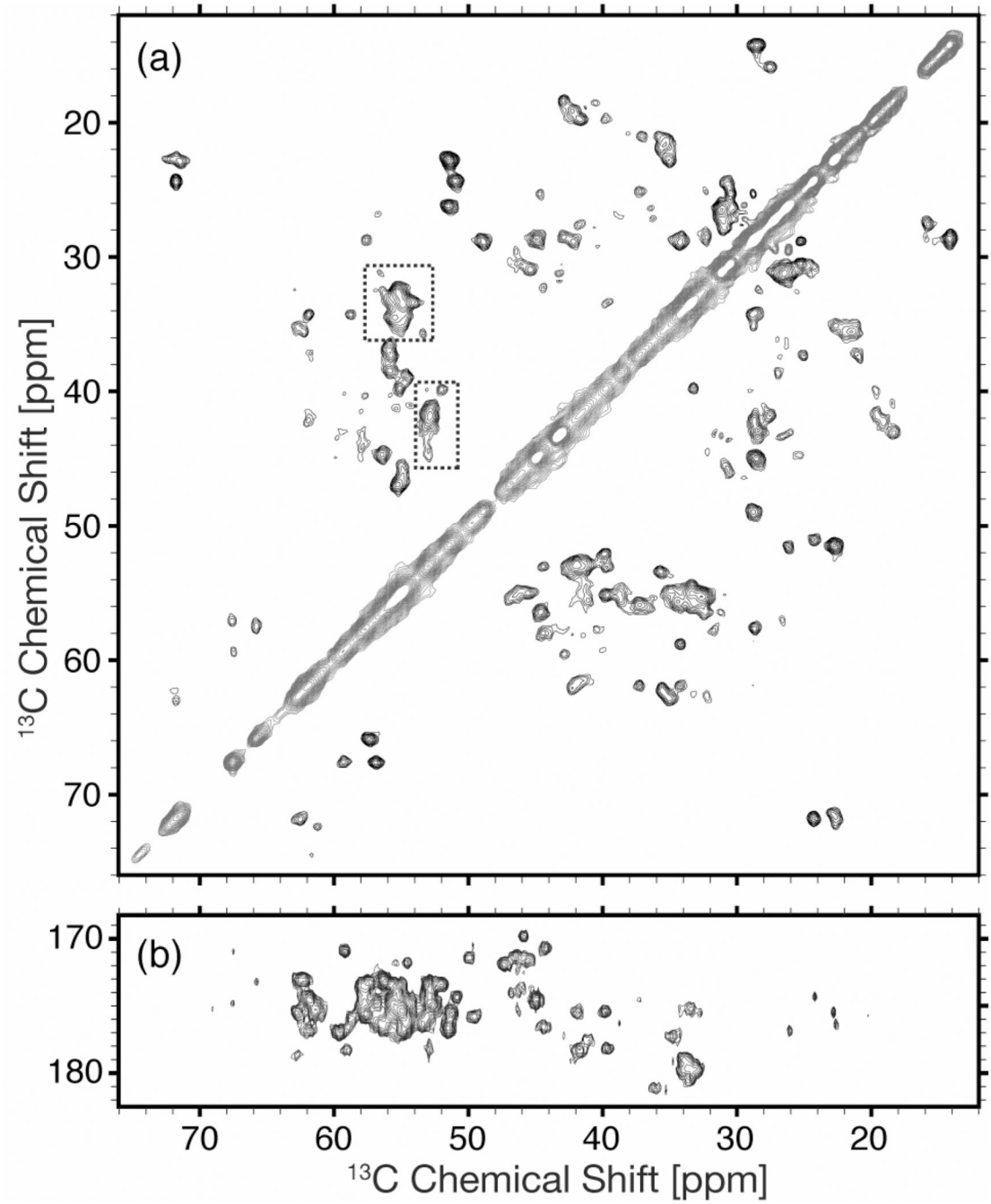

Figure 2.
2D ^{13}C-^{13}C correlation spectra of U-PI3-SH3 (750 MHz ^{1}H Larmor frequency, T = 2 °C). (a) Aliphatic region of a CMAR spectrum (2 ms mixing time, $\omega_r/2\pi$ = 28.571 kHz). Areas with high spectral overlap are indicated. (b) Carbonyl-aliphatic region of RFDR (1.76 ms mixing time, $\omega_r/2\pi$ = 18.182 kHz).

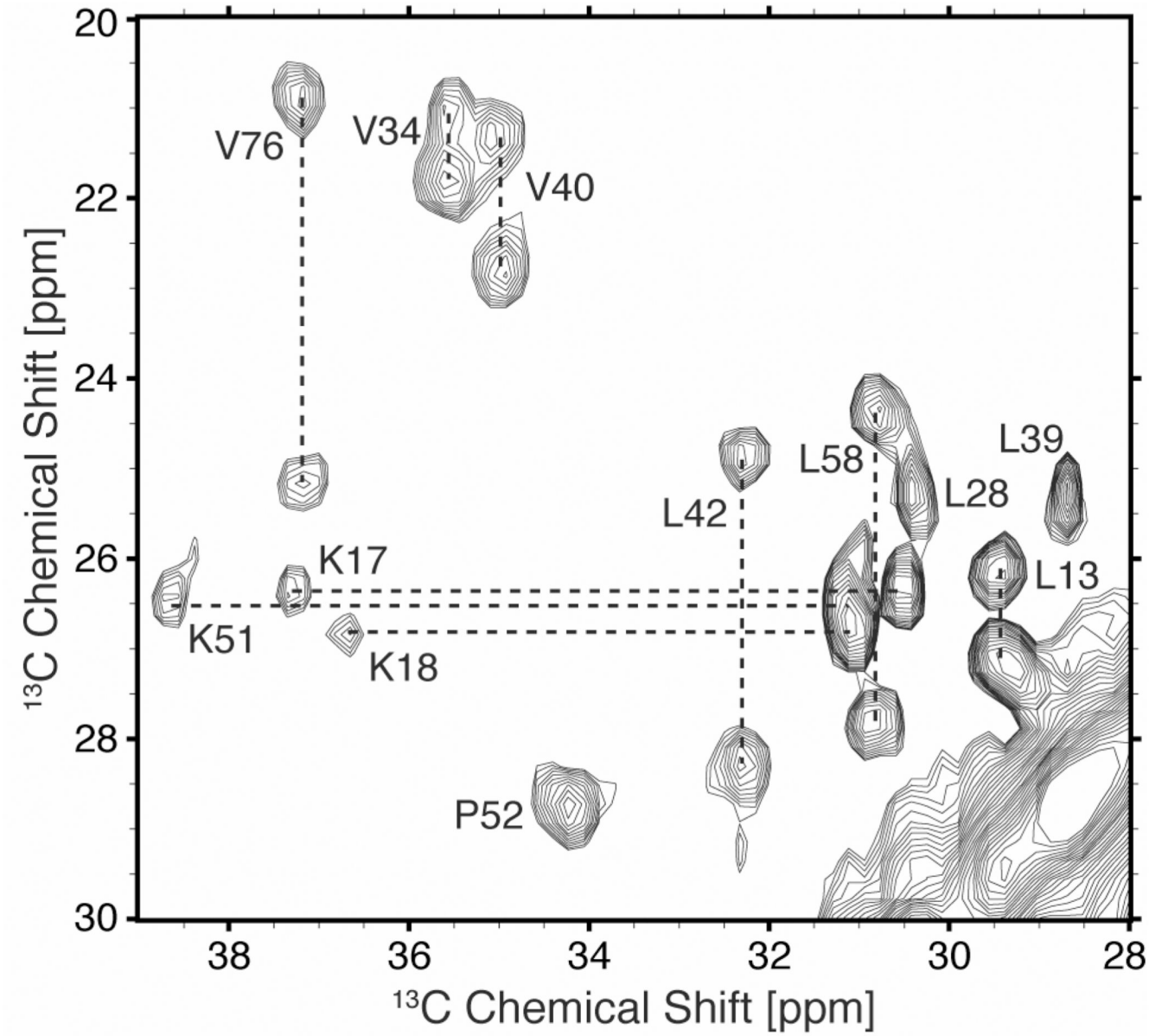

Figure 3.

Section of a 2D ^{13}C-^{13}C RFDR (1.76 ms) spectrum of U-PI3-SH3 illustrating aliphatic side-chain correlations, recorded at 750 MHz ^{1}H Larmor frequency, T = 2 °C, and $\omega_r/2\pi$ = 18.182 kHz. Typical line widths are between 80 and 115 Hz (0.4 to 0.6 ppm).

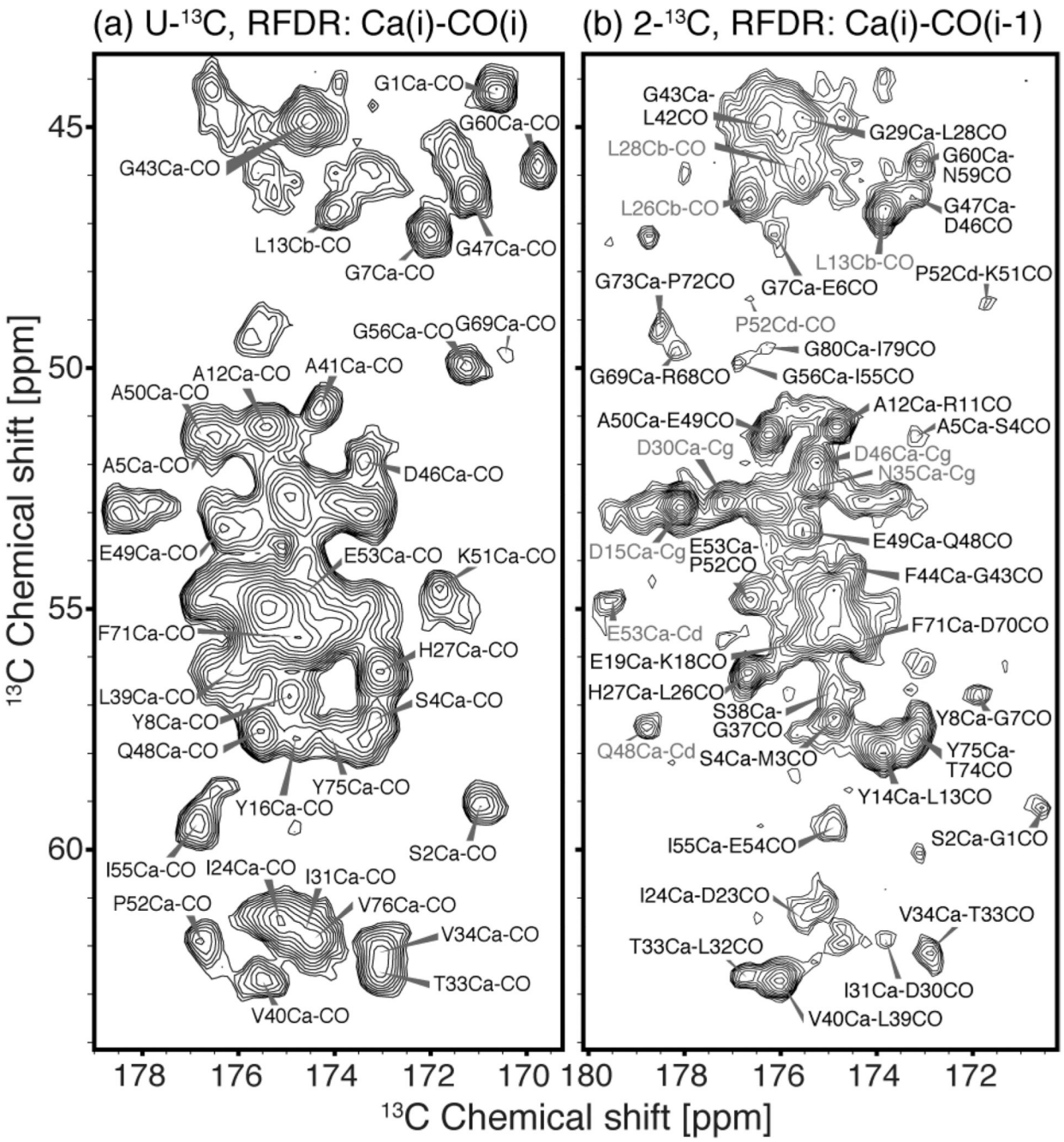

Figure 4.

Comparison of cross-peak information attainable in broadband Cα-C' correlation spectra of U-PI3-SH3 and 2-PI3-SH3. (a) Cα-C' region of a U-PI3-SH3 spectrum recorded with RFDR 2.24 ms mixing, displaying intra-residue one-bond correlations, some of which are labeled. (b) Similar region of a 2-PI3-SH3 spectrum recorded with RFDR 6.72 ms mixing, presenting multiple inter-residue two-bond correlations, labeled in black, and two-bond intra-residue correlations, labeled in gray. Both spectra were recorded at $\omega_r/2\pi$ = 28.571 kHz employing $\omega_1/2\pi$ = 120 kHz ^{13}C π pulses and without ^{1}H decoupling during the mixing period.

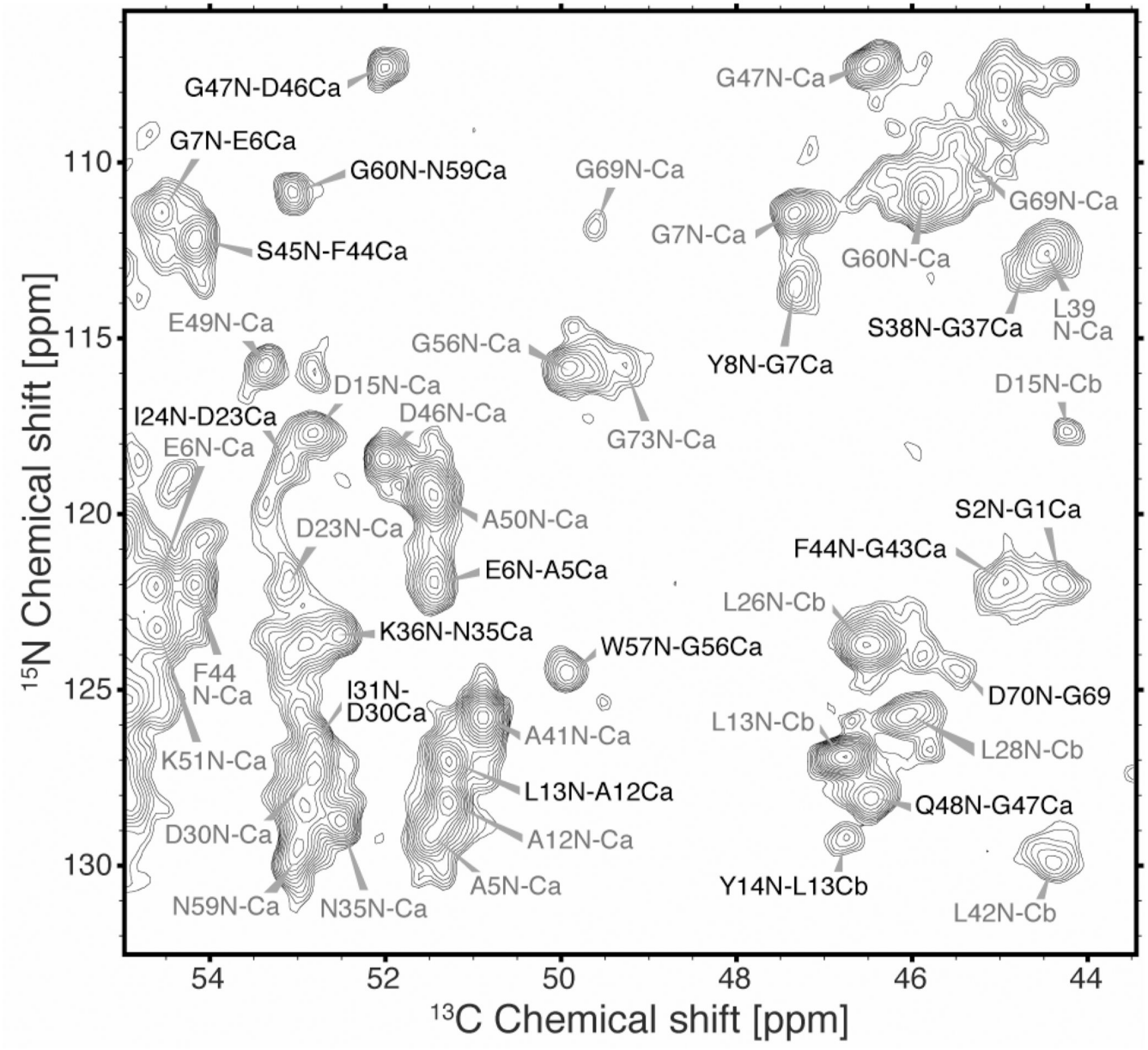

Figure 5.

Section of a TEDOR spectrum of 2-PI3-SH3 optimized for two-bond ^{15}N-^{13}C transfer with a 6 ms mixing period, recorded at $\omega_r/2\pi$ = 10 kHz and 700 MHz ^{1}H Larmor frequency. Sequential correlations are labeling in black and intra-residue cross-peaks are labeled in gray.

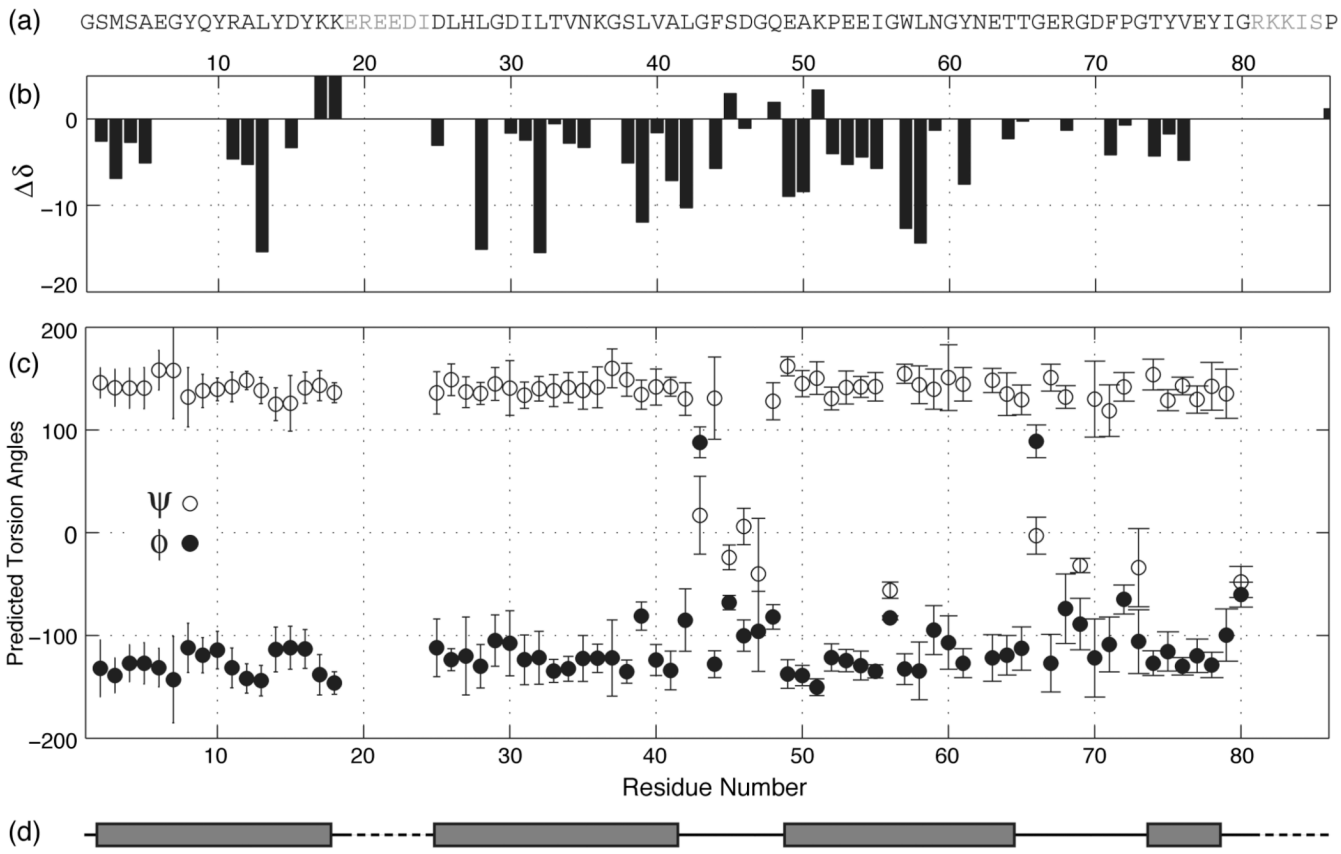

Figure 6.

Chemical shift analysis. (a) PI3-SH3 sequence, displaying unambiguously assigned (black) and unassigned (gray) residues. (b) Secondary structure propensity derived from the Chemical Shift Index, where negative numbers indicate a β-sheet conformation. (c) Backbone torsion angles (φ and ψ) predicted from ^{13}C and ^{15}N chemical shift analysis using TALOS. (d) Secondary structure diagram of the PI3-SH3 polypeptide chain in amyloid fibril form. Gray bars indicate regions of high β-sheet content, while a single line indicates a random coil conformation. Dash lines mark the positions of dynamic/disordered residues.

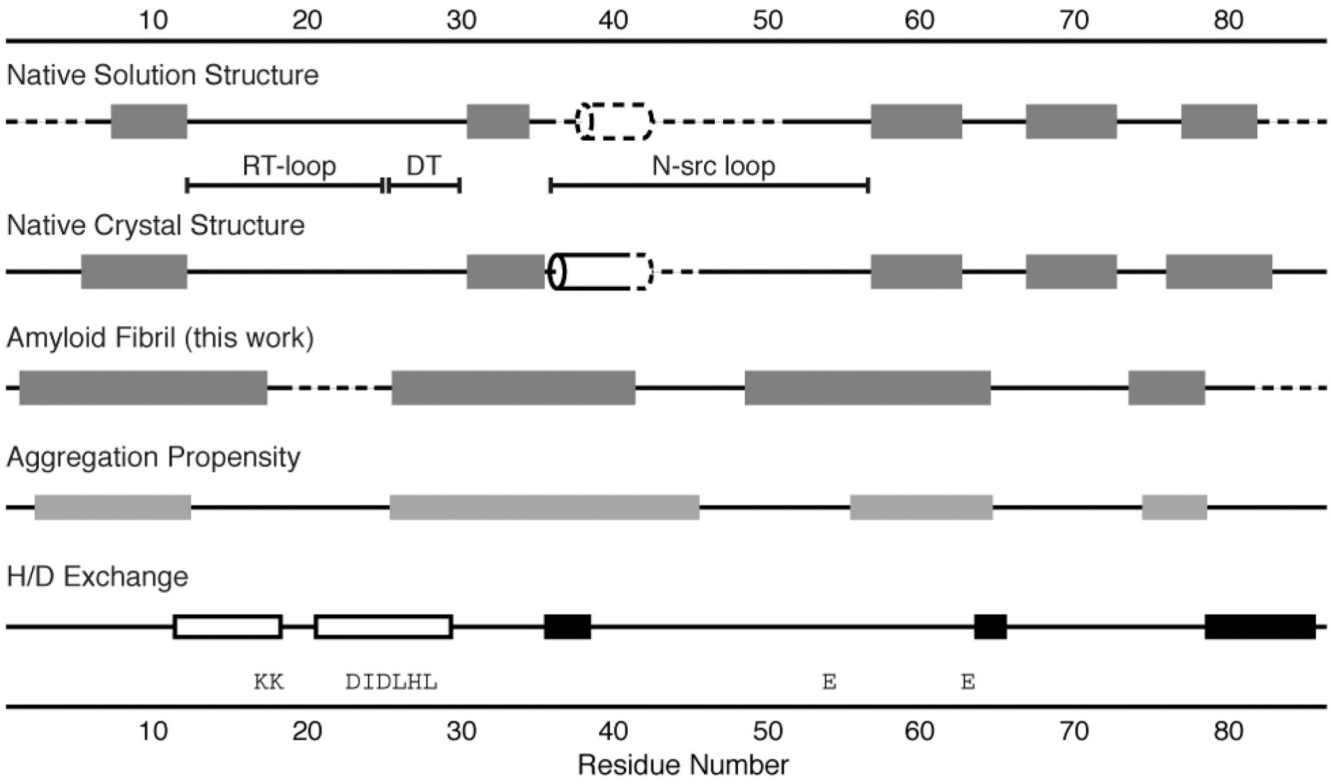

Figure 7.

Secondary structure of PI3-SH3 amyloid fibrils in the context of previous structural and mechanistic studies. From top to bottom: Secondary structure of natively folded PI3-SH3 in solution [Refs. 15 and 16] and in crystalline form [Ref. 14], with flexible regions shown with dashed lines, and the RT-loop, DT, and N-src loop, discussed in the text, are marked; secondary structure of PI3-SH3 in fibril form (from Figure 5d); aggregation propensity of the PI3-SH3 amino acid sequence [Ref. 75]; H/D exchange results showing highly protected regions (empty rectangles) and unprotected sites (filled rectangles). A few specific residues discussed in the text are also shown.

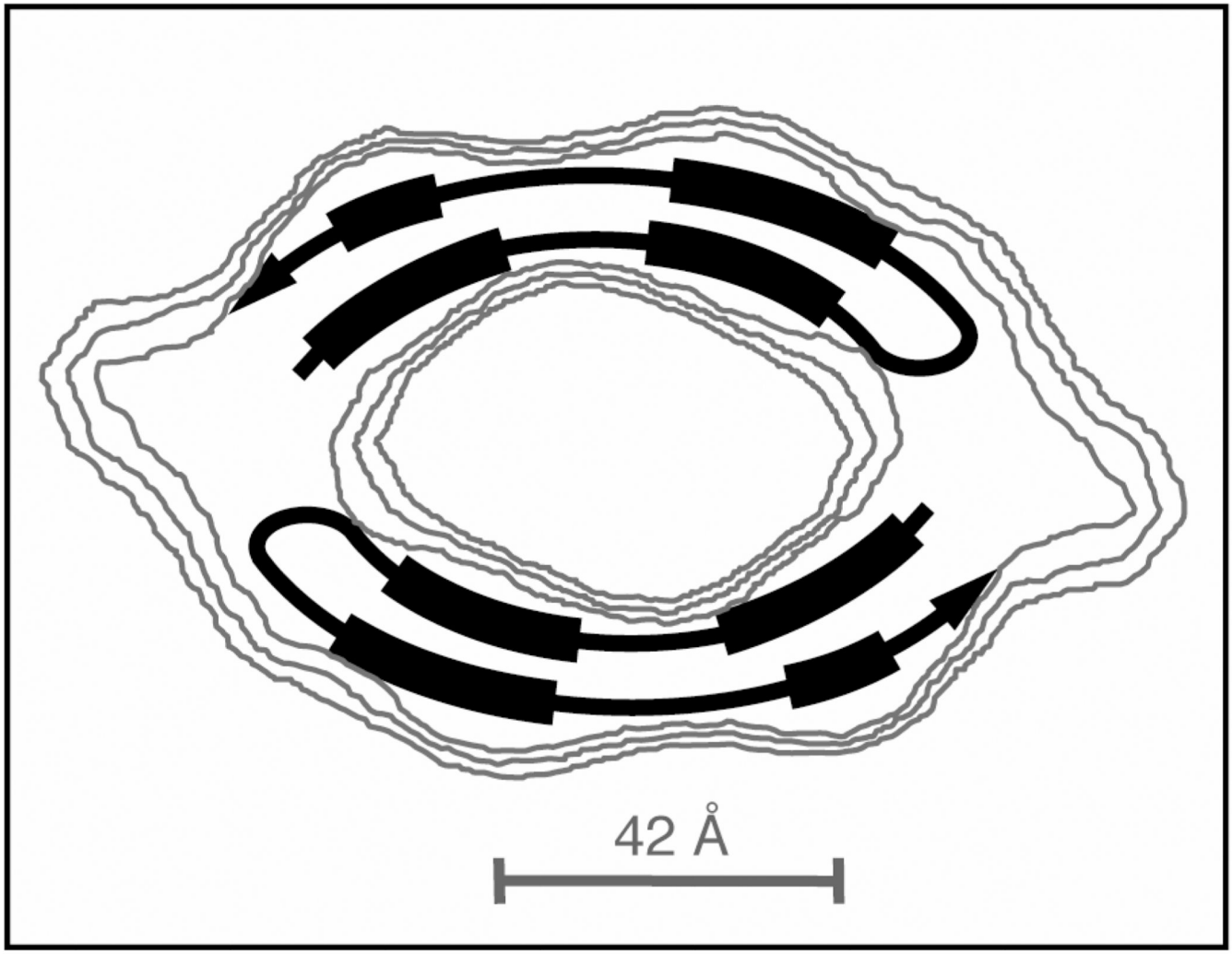

Figure 8.
Possible model for PI3-SH3 amyloid fibril architecture. The polypeptide chains are shown as single lines, with the thick segments denoting β-sheets running into the plane of the page, and are superimposed onto the cryo-EM map (adapted from Ref. 20) so that each protein subunit occupies one half of the fibril cross section. An arrowhead indicates the C-terminus.